Joanna Wojewoda, Paweł Zięba
Institute of Metallurgy and Materials Science
Polish Academy of Sciences, Kraków

THE ROLE OF INTERMETALLIC PHASES IN LEAD-FREE JOINING TECHNOLOGIES

Key words

intermetallic phases, diffusion soldering, isothermall solidification, growth rate constant, diffraction patterns, EDX analysis

Abstract

Paper reports the modern joining method called diffusion soldering. The process provides many advantages like, low joining temperature, high thermal stability of the interconnections and easy modus operandi. The essential effect, the formation of the intermetallic phases in the interconnection region, is described. The chemistry, microstructure and mechanical properties of the intermetallic phases appearing in the investigated interconnections, which could successfully replace the commonly used Pb-Sn solders are presented.

Streszczenie

W pracy opisano nowoczesną metodę spajania nazywaną lutowaniem dyfuzyjnym. Zaletami procesu są między innymi niska temperatura łączenia materiałów, wysoka stabilność temperaturowa powstałego złącza i zaskakująco prosta metodyka. Powstawanie faz międzymetalicznych jest warunkiem koniecznym do prawidłowego przebiegu procesu. Podano przykłady najbardziej znanych typów połączeń, które z powodzeniem mogą stać się

zamiennikami powszechnie stosowanych lutów Pb-Sn. Charakterystyka złączy zawiera opis ich mikrostruktury, składu chemicznego i właściwości mechanicznych.

1. Introduction

Solder joint is an essential part of electronic devices since it provides both electrical connection and mechanical bond. In most cases, the intermetallic phases (IPs) form and grow during soldering by the reaction between solder and metallic substrates. During conventional soldering a thin and continuous IP layer is an essential requirement for good wetting and bonding, and it improves the mechanical and electrical properties of such joint. On the other hand, too thick IP layer at the solder/conductor interface or unexpected morphological change may degrade the reliability of the solder joint [1,2].

Nowadays, the issue of joint reliability and performance is still a hot topic. The first reason stems from the Directive 2002/95/EC of the European Commission [3] which requires that the new electrical and electronic equipment should be free of lead and other hazardous substances by July 1st, 2006. The soldering, involving the use of suitable replacements, like tin-based multicomponent alloys with alloying elements such as Bi, In, Ag and Zn, leads also to the formation of intermetallic phases in the joined substrates. This obviously stimulates the research in this field [4,5].

Moreover, the operating temperature of many electronic devices built on silicon carbide and III-V compound semiconductors exceeds in many cases 350 °C. These high temperature devices find numerous applications

in jet engines, nuclear reactors, geothermal walls, automotive electronics, industrial robots, and space electronics.

Further, progressive miniaturization of components and contact areas in electronic packaging increase the specific load of contacts due to heat dissipation. Heat dissipating power components such as chip resistors and resistant heating elements cannot be connected to leads using a conventional soldering process. This results mainly from the fact that working temperature of the soft soldered joints is 60-100 °C below the soldering temperature (for the Pb-Sn solders the soldering temperature ranges from 220 to 260 °C).

2. Diffusion soldering

One of the promising techniques, which has a large potential to be applied for the fabrication of thermally and mechanically stable bonds, is diffusion soldering. It is based on the principle of isothermal solidification [6–10]. This is schematically presented in Fig. 1 for a hypothetical binary phase diagram containing two intermetallic phases (Fig. 2).

A low-melting material (LM) is sandwiched between high-melting materials (HMs). The sandwich can be accomplished by coating of the HM components with a thin LM layer (Fig. 1a) or using a thin-foil interlayer of LM. The assembly is clamped and then heated up from room temperature to the melting temperature of the LM (T_m), *heating stage*. Upon heating, interdiffusion may occur between the LM and HM

at the LM/HM interface. However, this is not so significant because usually the heating rate is very high.

Upon further heating up to the temperature of joining, T_j, the interlayer of LM is melt and part of the HM is dissolved into the liquid, *dissolution stage* (Fig. 1b). The width of the liquid zone increases and reaches its maximum at the end of the dissolution stage. After a certain time the composition of the liquid reaches C_L (Fig. 2).

Subsequent holding of the assembly at T_j, for a specified time and under a certain pressure p, leads to saturation of the liquid. At this moment a precipitation reaction takes place, most probably at the interfaces between the liquid and the substrates. The so-called *isothermal solidification* stage begins. The process can be controlled by diffusion of LM atoms into the solid HM. As local equilibrium at the precipitate/liquid interface is assumed, the concentrations at these interfaces are C_L and C_S, respectively (Fig. 2). The width of the liquid zone shrinks gradually, until the whole liquid is solidified. The joint formed consists of an intermetallic phase IP_1 (Fig. 1c).

As soon as the whole liquid is consumed, upon further annealing at T, solid-state interdiffusion takes place and the interconnection zone is enriched with HM atoms. After a certain time the change in composition promotes the formation and growth of another intermetallic phase IP_2 (Fig. 1d). The compositions at the interfaces between both IPs are C_1 and C_2 (Fig. 2). This is the final stage, called *growth of intermetallic phases*. Successively formed IPs with increasing concentration of HM are formed depending on the specific alloy system. In some circumstances two IPs can also coexist with unconsumed liquid [11].

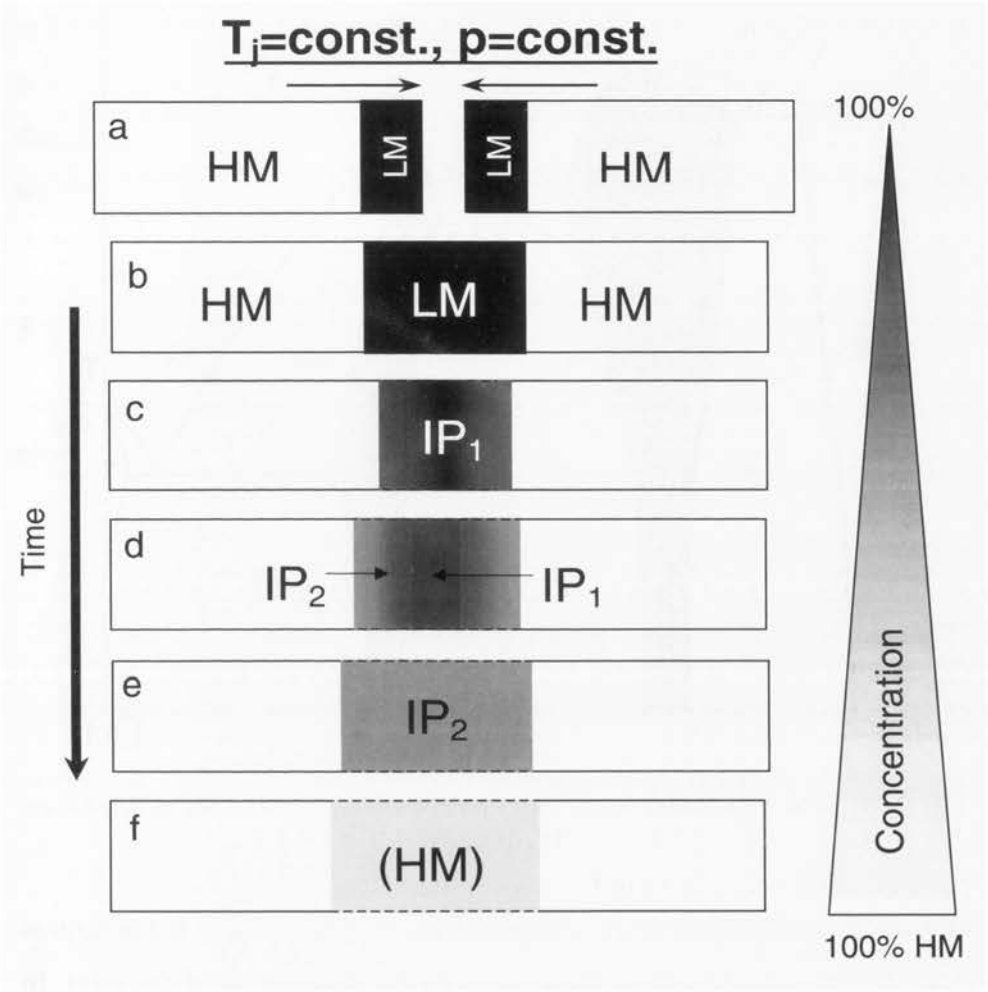

Fig. 1. Schematic diagram illustrating diffusion soldering. LM and HM are low and high melting components, respectively. IP_1 and IP_2 are successive intermetallic phases. The concentration of LM and HM components within the intermetallic phases are indicated on the concentration triangle

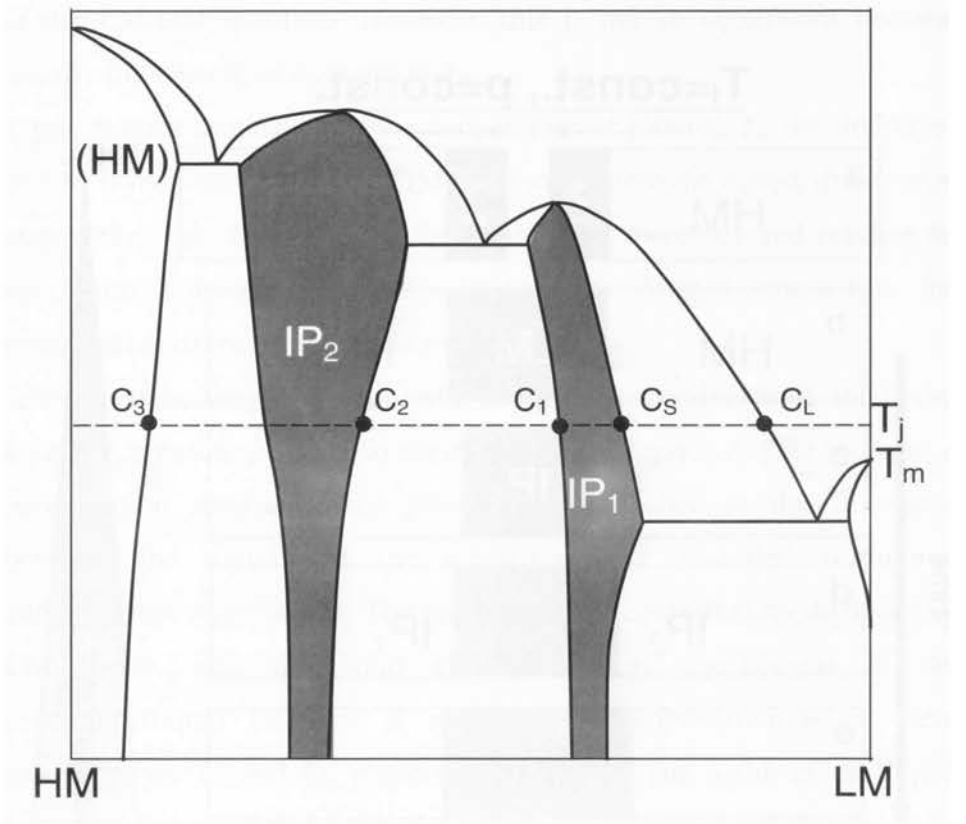

Fig. 2. Hypothetical binary phase diagram containing two intermetallic phases IP_1 and IP_2

The intermetallic phases are characterized by the melting temperatures much higher than the temperature used for the fabrication of the joint. In this way, the joint features advantageous intrinsic properties of the IPs, in particular high thermal and mechanical stability. The joint is also extremely thin, usually less than several microns, which adds to the mechanical properties and it facilitates the fabrication of electronics [1,12, 13].

Referring to other joining methods one can say that the diffusion soldering is a hybrid, which combines the advantages of conventional soldering (good joint filling and tolerance to surface preparation) and diffusion bonding (higher service temperature, smaller thermal expansion mismatch stresses).

3. Selection criteria for diffusion soldering

The potential candidates for diffusion soldering of electric and electronic devices should satisfy the following requirements:

1. They should form the thermally and mechanically stable joint at least up to 400-600 °C or even more.
2. The fabrication temperature should limit the thermal load exerted on the components during joint formation.
3. The isothermal solidification must be completed in relatively short time to enable the efficient use of the production line.
4. The simultaneous manufacturing of large number of joints with small dimensions must be possible.
5. They should ensure the economical repairing and recycling.
6. The joining process must be tolerant to the presence of oxide layer at a faying surface.

In principle, there is a wide selection of possible material combinations, but those which have been used recently, are listed in Table 1. The second important factor in designing of the solder (filler) material is its melting point. Especially, in the microelectronic industry, the Si/Si

interconnection requires to use the low-melting point materials. Referring to Table 1 one can see that tin is frequently used as it is characterized by melting point close to the conventional Pb-Sn solder. Lowering of the soldering temperature by 50 deg can be obtained by replacing tin by indium. Further lowering is attributed to the implementation of eutectic In-Sn alloy.

Table 1. Recently used combinations of metals for binary and ternary joints

Binary joints	
Cu/In/Cu	Ni/Sn/Ni
Cu/Sn/Cu	Ni/Al/Ni
Ternary joints	
Cu/In-48at.%Sn/Cu	
Cu/Bi-22at.%In/Cu	

Table 2. Low-melting-point alloys which can be used as fillers in diffusion solde- ring process

No.	Element (wt.%)			T_M [°C]
	A	B	C	
1	In(51)	Bi(33)	Sn(16)	61
2	In(62)	Bi(34)	---	72
3	In(26	Bi(57)	Sn(17)	79
4	In(33)	Bi(67)	---	109
5	In(52)	Sn(48)	---	118
6	Sn(42)	Bi(58)	---	138
7	In	---	---	156
8	Sn(91)	Zn(9)	---	199
9	Sn	---	---	232
10	Al	---	---	660

However, the lowest melting point solder which was successfully applied is eutectic Bi-In alloy. An exception is Ni/Al/Ni joint as aluminium possesses relatively high melting point. However, in this particular case the joint is designed not for electronics but for electrotechnics where thermal stability, as much high as possible, is required.

4. Formation of intermetallic phases in selected diffusion-soldered interconnections

4.1. Cu/Sn/Cu interconnection

The Cu-Sn system is also suitable for the diffusion soldering because at the soldering temperature slightly above the melting temperature of Sn (T_m= 232 °C) the η(Cu_6Sn_5) and ε(Cu_3Sn) intermetallic phases form (Fig. 3). Thus, the joint containing Cu_6Sn_5 is thermodynamically stable up to 415 °C.

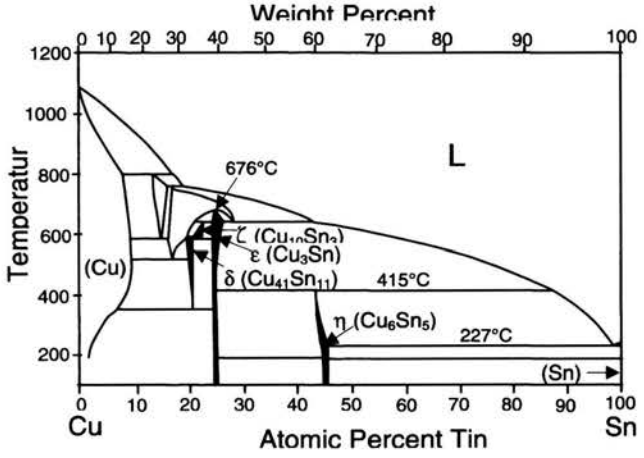

Fig. 3. Simplified version of Cu-Sn equilibrium phase diagram based on data of Saunders and Miodownik [14]

Recently, the Cu/Sn/Cu interconnections have been investigated by Gust et. al. [15, 16] and Jacobson and Sangha [17]. Figure 4 presents optical microscope (LM) images of the joint obtained at relatively low temperature of 240 °C [15]. The η and ε phases form almost simultaneously (Fig. 4a). However, the growth velocity of the η phase is

very fast compared to that of the ε phase. The η phase appears in the shape of single crystals hemispheres. The deep grooves existing between hemispheres were considered by Bader, Gust and Hieber [15] to be important diffusion paths for Cu and Sn in addition to the bulk diffusion through the η phase. After 8-10 min all the tin is completely converted into IPs. Then the η phase transforms into the ε phase according to the scheme:

$Cu_6Sn_5 + 9Cu \rightarrow 5\ Cu_3Sn.$

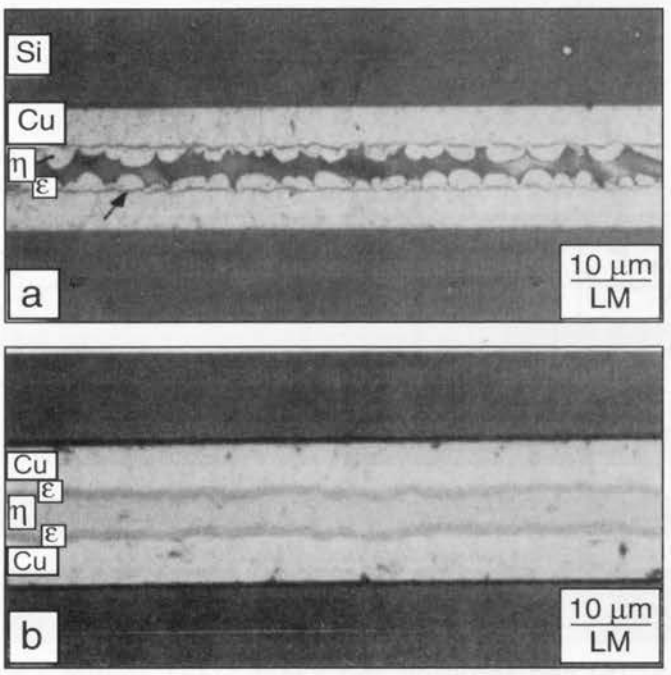

Fig. 4. Images of Cu/Sn/Cu interconnection diffusion soldered at 240 °C [15]. Cu/5.2 μm Sn/Cu after 1 min (a). Cu/3.2 μm Sn/Cu after 20 min of reaction (b). Tin in (a) was selectively etched away

The resulting phase is characterized by much better physical properties than Cu_6Sn_5. If the Sn interlayer is sufficiently thin, the joint can transform to Cu-solid solution after several minutes of annealing just below 600 °C [17]. The tensile test revealed that the strength of the joint containing both IPs is almost twice higher than for pure Sn (18 MPa) [16].

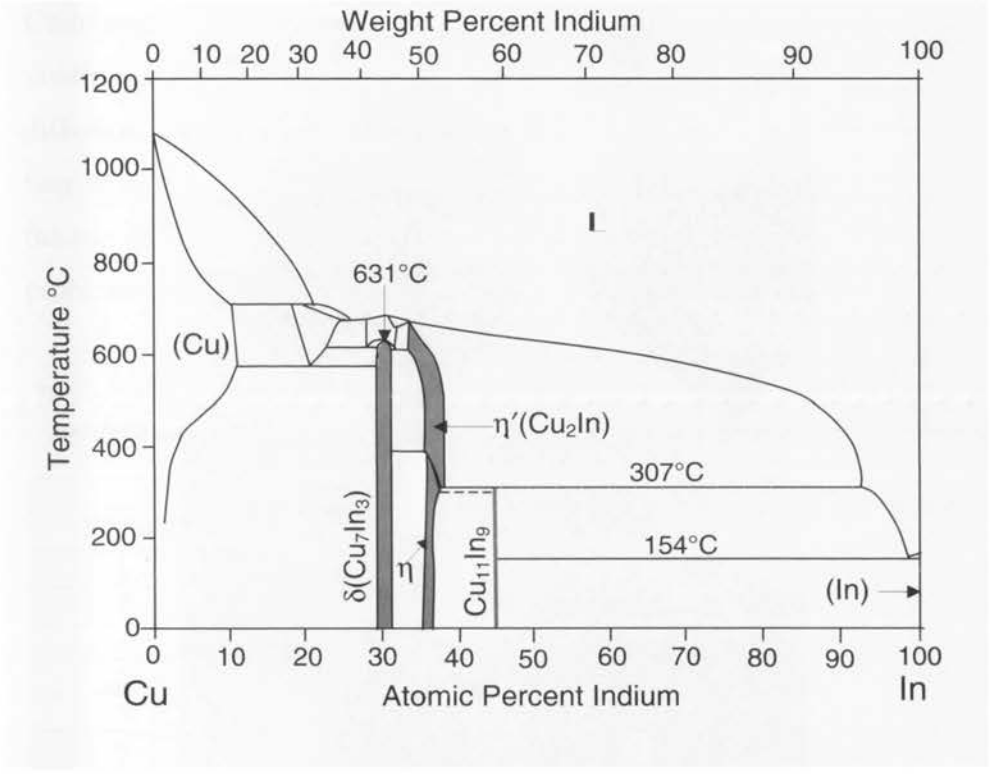

Fig. 5. Simplified version of Cu-In equilibrium phase diagram based on data Subramanian and Laughlin [18]

4.2. Cu/In/Cu interconnection

Three intermetallic phases are present in the Cu-In equilibrium phase diagram (Fig. 5). The first one, $Cu_{11}In_9$ forms below 307 °C while others $\delta(Cu_7In_3)$ and $\eta(Cu_2In)$ are stable above this temperature.

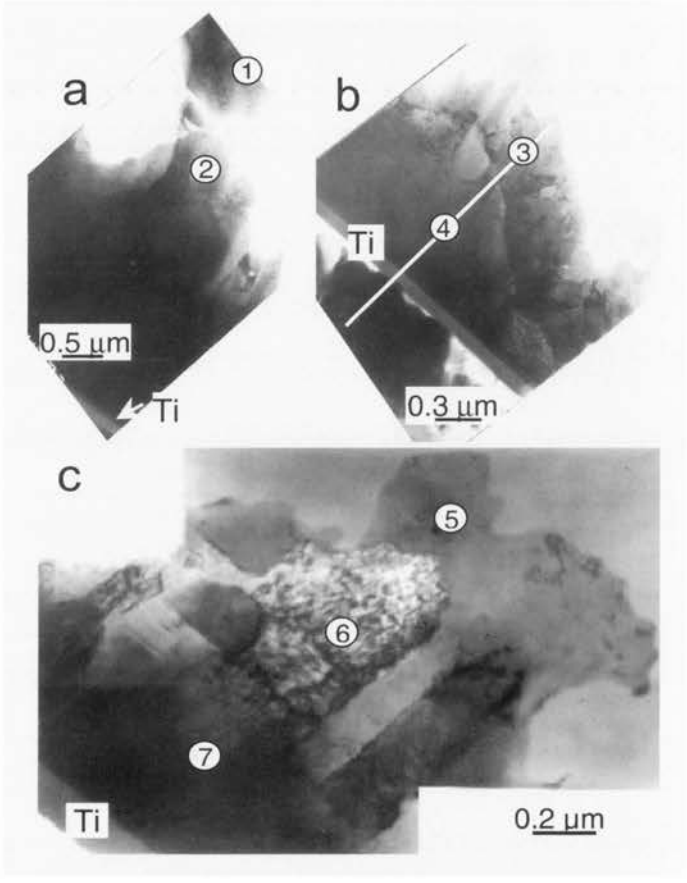

Fig. 6. TEM micrographs (a-c) of a Si/Cu/In/Cu/Si interconnection after 240 s at 180 °C. Numbers in white circles are the places where selected area electron diffractions were taken (see Table 3)

Figure 6 presents a transmission electron microscopy (TEM) micrographs of the Si/Si interconnections, obtained using a Cu metallization and an In interlayer and joined by diffusion soldering at 180 °C [19, 20]. In the microelectronic industry, silicon is used in conjunction with a SiO_2 interlayer in order to reduce the capacitance and resistance of the interconnection in an integrated circuit. It has to be metallized with Cu to avoid deterioration of the device due to electromigration and stress voiding. However, one of the major drawbacks of Cu coating is the fast diffusion of the Cu atoms in Si and drift in SiO_2. Hence, a diffusion barrier is necessary between Cu and Si or SiO_2 which is accomplished by the use of Cr, Ti or W or complex compounds [21]. This also reduces the problem of thermal-expansion mismatch stresses.

Table 3 Phase identification based on selected-area electron diffraction (SAD) patterns and quantitative point EDX analysis in areas indicated in Fig. 6

SADP	Phase identified	In (at.%)
1	η (Cu_2In)	35.9
2	η (Cu_2In)	35.2
3	δ (Cu_7In_3)	29.4
4	Cu	0.4
5	η (Cu_2In)	36.3
6	η (Cu_2In)	34.7
7	Cu	0.1

The quantitative energy dispersive X-ray (EDX) analysis performed along a solid line in Fig. 6b indicated that the first layer adjacent to Ti diffusion barrier, was still unreacted copper, although most of the indium has already been transformed into η(Cu_2In) intermetallic phase

containing 34.7-36.3 at.% In. In some places (Fig. 6b) the reaction was in more advanced stage associated with the formation of the $\delta(Cu_7In_3)$ phase according to the reaction: $3Cu_2In + Cu \rightarrow Cu_7In_3$.

The obtained results agree with the thermodynamic considerations. The lack of $Cu_{11}In_9$ says that this phase has already been consumed by the growth of the two other intermetallic phases. However, applying 20 μm In foil instead of 1.5 μm magnetron sputtered layer allows to detect the $Cu_{11}In_9$ after even 30 days at 180 °C [20].

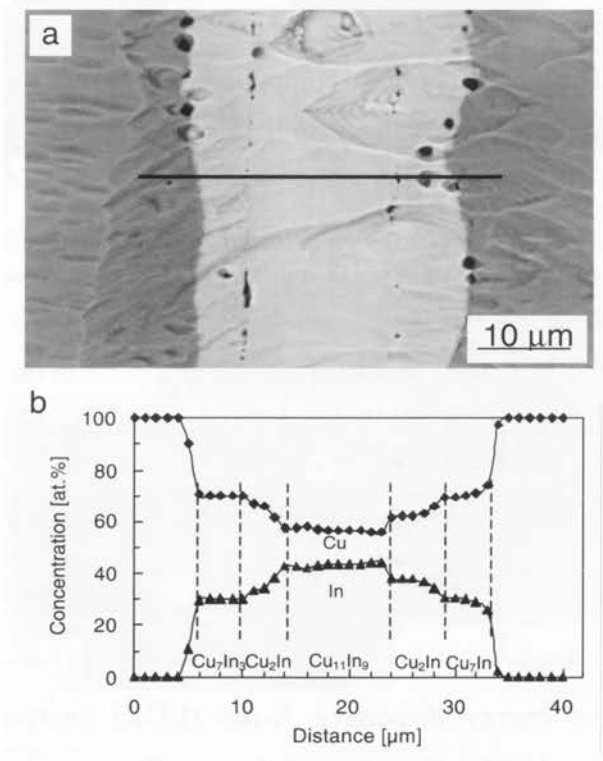

Fig. 7. (a) SEM micrograph of a Cu/In/Cu joint after 16 days of reaction at 290 °C and (b) corresponding EDX analysis results for Cu and In along the line in Fig. 7a

A scanning electron microscopy (SEM) micrograph showing the cross-sectional view of the Cu/In/Cu interconnection after 16 days of reaction at 290 °C is presented in Fig. 7a. The bright, central part is the joint while the right and left layers are the Cu subshates. The EDX analysis across the joint revealed three distinct areas corresponding to the intermetallic compounds $Cu_{11}In_9$ -(45 at.% In), $\eta(Cu_2In)$-37 at.% In and $\delta(Cu_7In_3)$-30 at.% In as seen in Fig. 7b. The absence of microcracks, voids, pores and other deformities indicates the good quality of the obtained joint at the interface between Cu/Cu_7In_3. Some defects are visible within the joint.

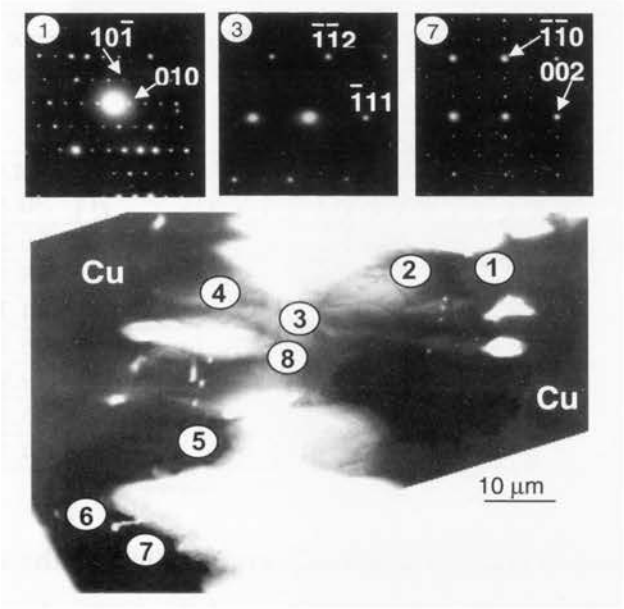

Fig. 8. TEM micrograph of a Cu/In/Cu joint after 16 days of reaction at 290 °C. Numbers in white circles are the places where selected area electron diffractions were taken. Above are SAD patterns taken at point 1 identified as δ(Cu_7In_3) with [101] zone axis, at point 3 identified as $Cu_{11}In_9$ with [312] zone axis, and at point 7 identified as η(C) phase with [1 1 0] zone axis

A number of selected area electron diffraction patterns (SADP) were taken from the joint zone. They are marked by numbers in white circles in Fig. 8. In each case, SADP was accompanied by EDX quantitative point analysis exactly at the same place where the diffraction pattern was obtained. The results of the investigation are summarized in Table 4. The diffraction patterns of the phases specified in Table 4 were obtained consistently and reproducibly and indicate the presence of three intermetallic phases in the joint; namely, $Cu_{11}In_9$, $\eta(Cu_2In)$ and $\delta(Cu_7In_3)$.

Table 4 Phase identification based on selected-area electron diffraction patterns (SADPs) and quantitative EDX point analysis in areas indicated in Fig. 8

SADP	The phase	In [at.%]
1	$\delta(Cu_7In_3)$	30.1
2	$\eta(C)$	36.2
3	$Cu_{11}In_9$	45.7
4	$Cu_{11}In_9$	44.3
5	$Cu_{11}In_9$	45.1
6	$\delta(Cu_7In_3)$	29.9
7	$\eta(C)$	35.3
8	$Cu_{11}In_9$	44.7

Some typical diffraction patterns corresponding to the centre of the joint on area close to the Cu substrate and the region located between them are also shown in Fig. 8. In the case of the η-phase ordering of the atomic arrangement of the high temperature hexagonal H phase [22] leads to many different, but closely related superstructures: A, B and C. For the A and B phases, the superstructure reflections are only observed

in directions perpendicular to the hexagonal c-axis of the parent H phase, whereas for the C-phase these reflections are also observed along the C-axis.

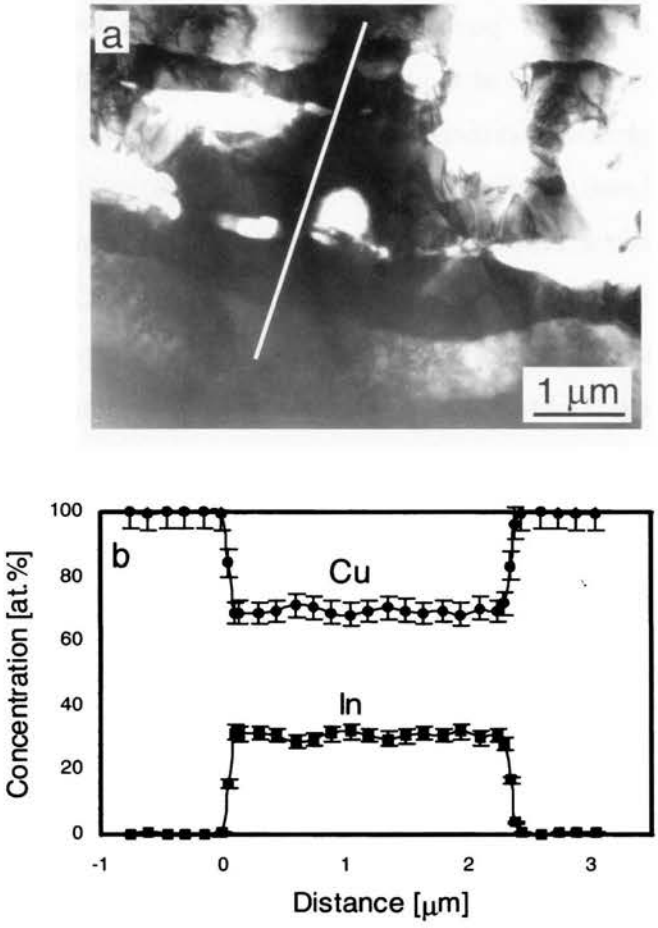

Fig. 9. (a) TEM image of Cu/In/Cu interconnection after diffusion soldering at 430 for 1.5 h; (b) Cu and In concentration profiles performed using EDX spectrometer along line indicated in Fig. 9a

The examined diffraction patterns are complicated and difficult to interpret. The strong reflections on η-type diffraction patterns were indexed using the parent hexagonal lattice (with a=0.428 nm; c=0.526 nm). In most cases positions of additional, weaker reflections on diffraction patterns are at the same positions as those shown in [22] and can be interpreted as orthorhombic C-phase (with a=3.839 nm, b=0.739 nm, c=2.097 nm), see Fig. 8.

Figure 9 shows a TEM image of a Cu/In/Cu joint annealed at 430 °C for 1.5 h. The presence of the only intermetallic phase $\delta(Cu_7In_3)$ containing 29-31 at.% In was proved by the quantitative EDX analysis and SADPs.

The SEM and TEM examinations combined with phase identification using EDX and electron diffraction analysis revealed the presence of three different intermetallic phases during the formation of Cu/In/Cu joints. These are: $\delta(Cu_7In_3)$, $\eta(Cu_2In)$ and $Cu_{11}In_9$. According to the equilibrium phase diagram (Fig. 5) two different phase fields exists depending on the temperature process. Above 307 °C two equilibrium intermetallic phases can form: $\delta(Cu_7In_3)$ and $\eta(Cu_2In)$. Below this temperature three intermetallic phases are possible: $\delta(Cu_7In_3)$, $\eta(Cu_2In)$ and $Cu_{11}In_9$. The experiments agree with these thermodynamic consideration. At 290 °C all the three phases were present. A previous study [20] at 180 °C revealed just two of them because the $Cu_{11}In_9$ phase was already consumed by the growth of the other two intermetallic phases. A similar situation occurred at 430 °C (Fig. 9) where the $\eta(Cu_2In)$ phase was consumed during growth of the $\delta(Cu_7In_3)$ containing

29-31 at.% In. The results of the present investigation indicate that in a Cu/In/Cu joint the following reactions take place:

9 In (liquid) + 11 Cu (solid) → $Cu_{11}In_9$; $Cu_{11}In_9 + 7\ Cu \rightarrow 9\ Cu_2In\ (\eta)$;

3 $Cu_2In\ (\eta) + Cu \rightarrow Cu_7In_3\ (\delta)$

The increase of the soldering temperature to 430 °C substantially accelerates the formation of the joint and avoids the formation of the $Cu_{11}In_9$ phase, which is stable only to 307 °C. The joint formed at 430 °C should benefit from the relatively low melting temperature of In (159 °C) and high thermal stability of the $\delta(Cu_7In_3)$ and $\eta(Cu_2In)$ intermetallic phases (up to 631°C). On the other hand, it should be remembered that Cu is used in electronic industry as a metallization layer on silicon substrates. Therefore, the temperature increase by 150 °C may have negative effects on the properties of silicon.

4.3. Cu/In-Sn/Cu interconnection

An overall view of the Cu/In-Sn/Cu joint is presented in Fig. 10. At least three different zones can be distinguished in the joint. They are separated by quite sharp interfaces marked with a dotted white line to make better visible. A closer inspection using selected area electron diffraction technique allowed for the conclusion that the η phase based on Cu_6Sn_5 existed in the central part of the joint. This phase appears both in Cu-Sn [14] and Cu-In [18] phase diagrams and it was difficult to distinguish, whether it is $\eta(Cu_6Sn_5)$ or $\eta(Cu_2In)$ intermetallic compound. Both phases have the same structure with similar lattice constants. An

additional test performed using EDX technique revealed that the composition in the middle of the joint is close to that appropriate for Cu_6Sn_5 compound (see Table inserted in Fig. 10a). With an increasing distance from the middle of the joint, the amount of In also increased replacing Sn. This promoted formation of the η phase based on Cu_2In.

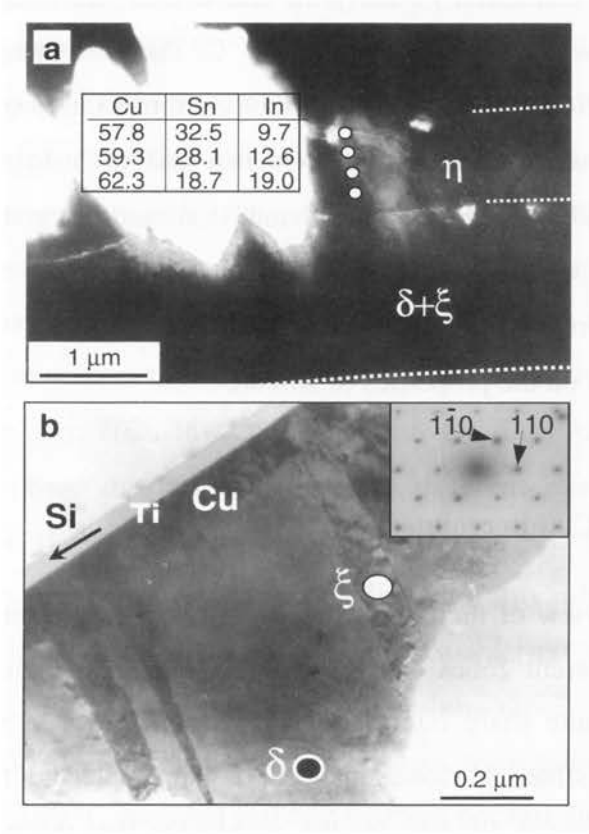

Fig. 10. TEM micrographs of Cu/Sn-In/Cu interconnection after 243 h of reaction at 200 °C: (a) Overall view of the joint showing points of EDX analysis and corresponding content of Cu, In and Sn (in at.%), (b) Outer zone of the joint where phases δ and ξ co-exist. The SAD pattern of ξ phase is also inserted

In the region next to copper, two intermetallic phases were detected. The first phase was located in the thin plates growing in perpendicular direction to the copper layer (Fig. 10b). One should note that according to the Cu-Sn phase diagram there is no large differences between chemical compositions of the $\delta(Cu_{41}Sn_{11})$, $\xi(Cu_{10}Sn_3)$ and $\varepsilon(Cu_3Sn)$ phases. They contain 79-80 at.% Cu, 77.5-79.7 at.% Cu and 74.1-75.5 at.% Cu, respectively. Taking into account the accuracy of the EDX analysis (for an experienced user and experimentally determined Cliff-Lorimer factors it is 4-7% relative) it was difficult to judge, which phase was present in contrasting strips shown in Fig. 10b. However, the SAD patterns (the example in Fig. 10b) taken in the areas like those indicated by an open circle showed convincingly the presence of ξ phase and not the ε phase.

On the other hand, the EDX analysis performed along the area between sharp-contrasting strips showed rather uniform distribution of elements to be: 69.4÷70.5 for Cu, 9.5÷10.3 for Sn and 19.6÷21.1 for In (all in at.%), which correspond rather to the δ phase based on the Cu_7In_3 compound.

4.4. Cu/Bi-In/Cu interconnection

There are three kinds of intermetallics in the equilibrium Bi-In phase diagram (Fig. 11). These are BiIn (35.5 wt% In), Bi_5In_3 (47.6 wt% In) and $BiIn_2$ (52.4 wt% In). It can be seen that BiIn is the highest melting intermetallics in the system and it melts congruently at 110 °C.

The eutectic In-Bi alloy as the interlayer was chosen because of its unquestionable advantage-the low melting temperature (only 72 °C). It was applied to join the copper substrates in the temperature ranging from 85 to 150 °C under a low pressure in the argon atmosphere.

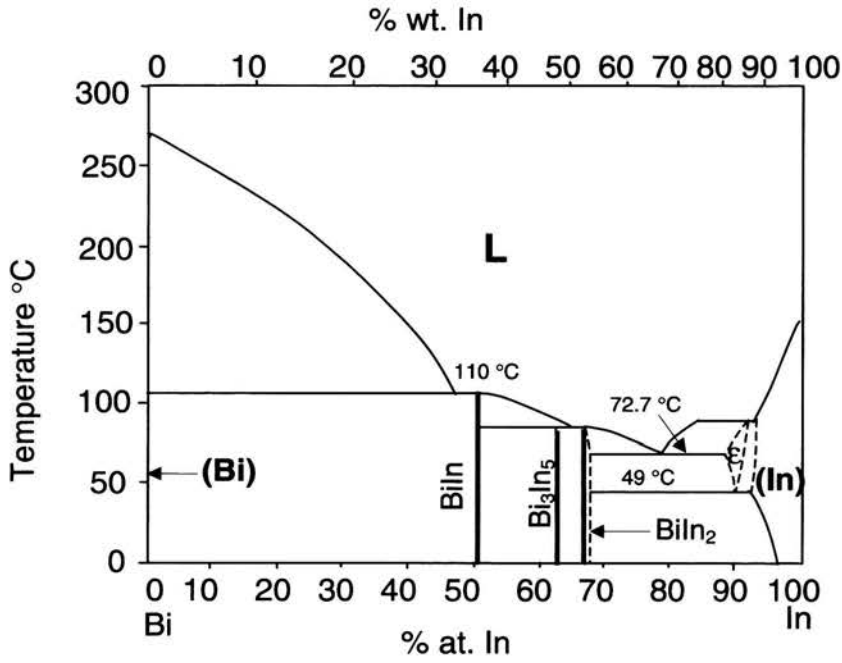

Fig. 11. Simplified version of In-Bi equilibrium phase diagram based on data [23]

Just 15 minutes of annealing at temperatures of 125 and 150 °C leads to the formation of the first intermetallic phase in the joint. The use of the SEM equipped with the EDX spectrometer allowed to identify it as $Cu_{11}In_9$ with melting temperature of 307 °C. Further annealing revealed that $Cu_{11}In_9$ forms rather homogeneous layer at lower reaction

temperatures (85 and 100 °C) while at higher ones (125, 150 °C) the hemisphere scallops were observed, see Fig. 12.

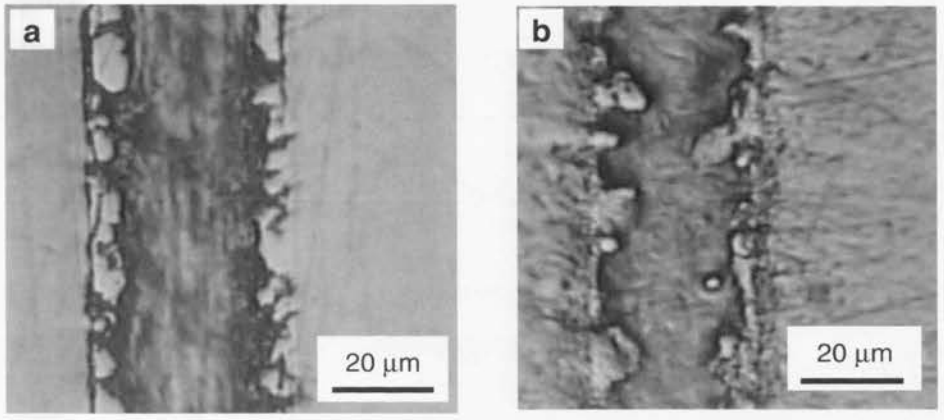

Fig. 12. The light microscopy microstructure of the interconnections annealed at the 125 °C (a) and 150 °C (b) for 1 hour

The mechanical properties of the phases were inspected using the NanoIndenter XP™ instrument. The load-displacement data provided the information about the hardness and the elastic-plastic deformation behavior of the phases. The indenter displacement in the Bi-In alloy was accommodated plastically (Fig. 13a) and the phase was found to be very soft (with the hardness value of 0.17 GPa). On the contrary, the intermetallic phase $Cu_{11}In_9$ response on the loading - unloading treatment had an elastic-plastic character (Fig. 13b). Consequently, the hardness was significantly larger (5.92 GPa). That means the $Cu_{11}In_9$ phase has the potential for brittle behavior. Also the elastic modulus was determined for the both phases BiIn and $Cu_{11}In_9$ and was equal to 34.1 and 103.5 GPa, respectively.

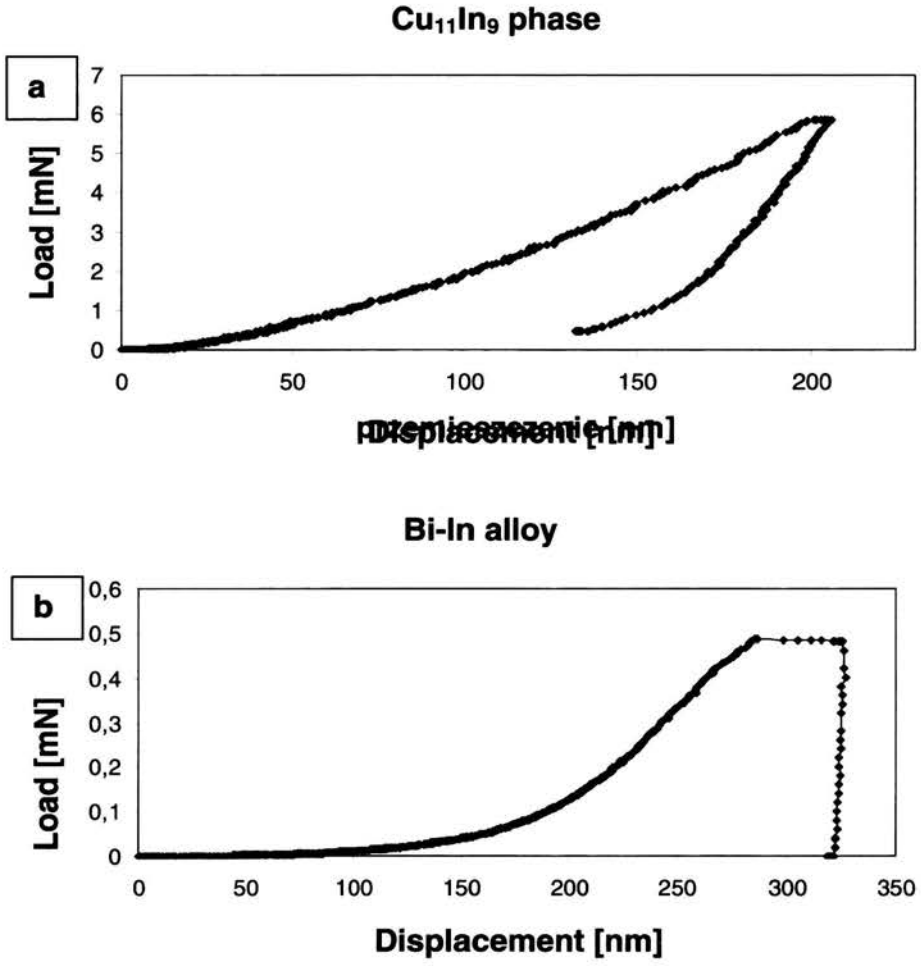

Fig. 13. Load-displacement curves describing obtained using performed on NanoIndenter XP™ for $Cu_{11}In_9$ phase (a) and BiIn alloy (b)

4.5. Ni/Sn/Ni interconnection

There are three intermetallic phases in the Ni-Sn system: Ni_3Sn_4, Ni_3Sn_2 and Ni_3Sn. They are stable up to 794, 1250 and 1174 °C. This feature along with relatively low melting point of pure tin (232 °C) allows to obtain thermal stability in the joint several times higher than the soldering temperature.

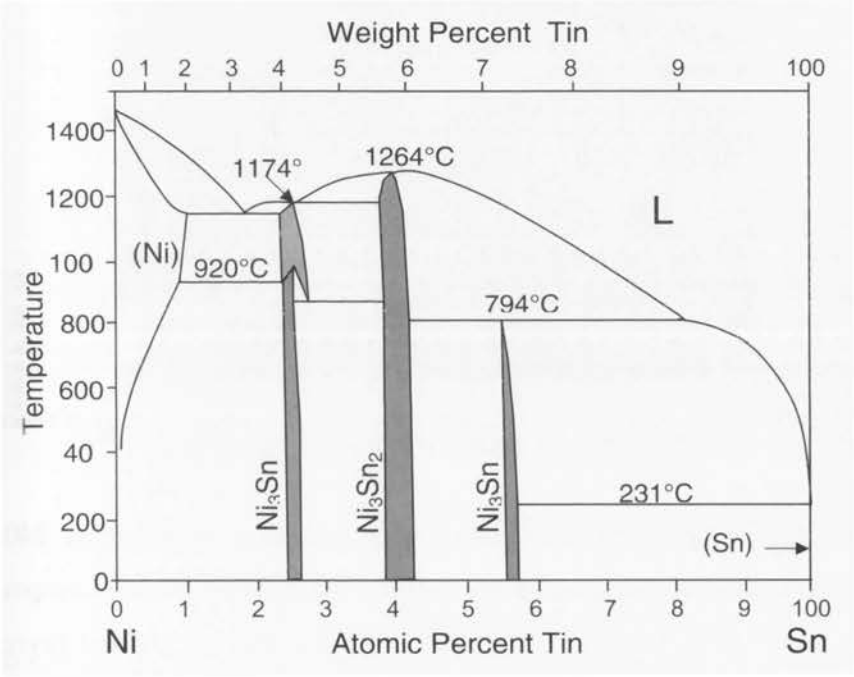

Fig. 14. Simplified version of Ni-Sn equilibrium phase diagram based on data of Nash [24]

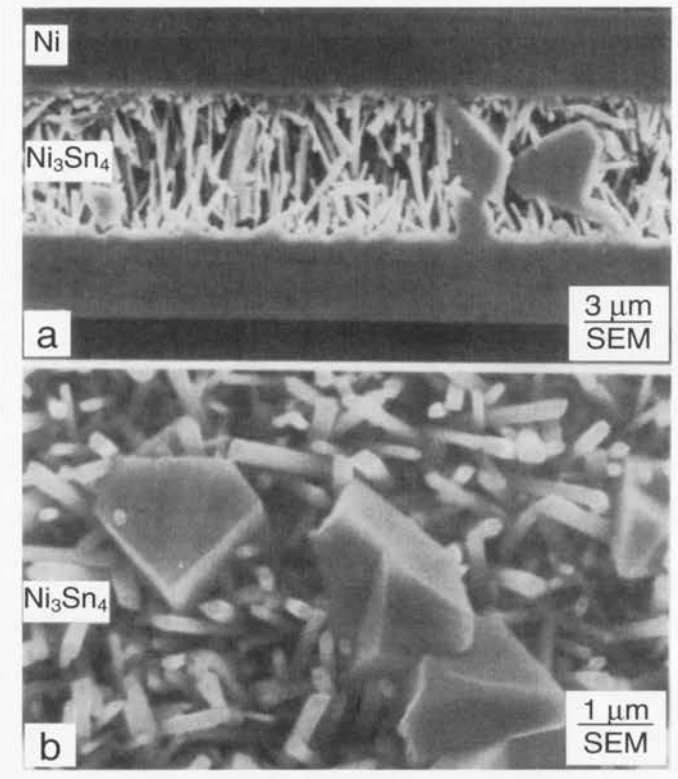

Fig. 15a-b. Ni/8.6 µm Sn/Ni interconnection after 165 s (a), 60 s (b) of reaction at 240 °C. [15]. Tin was selectively etched away

Figure 15a-b shows Ni/Sn/Ni joint after diffusion soldering at 240 °C [15]. Short time of the reaction leads to the creation of Ni_3Sn_4 compound, only. Sufficiently long time of reaction results in fine grained layers at the Ni interface and a coarse grained area in the middle (Fig. 15a). The quick growth, the idiomorphic shape of big crystals indicated that the Ni_3Sn_4 initially formed almost exclusively by the diffusion of Ni through the liquid Sn and crystallization from the liquid phase.

Along with the time of reaction the transport capacity of the diffusion paths through the liquid Sn decreased because of the growing density of

solid phase. The Ni_3Sn phase appeared almost simultaneously with Ni_3Sn_2 phase at 300 °C (Fig. 15b). When Ni_3Sn did not form, the Ni/Ni_3Sn_2 interface was mechanically weak.

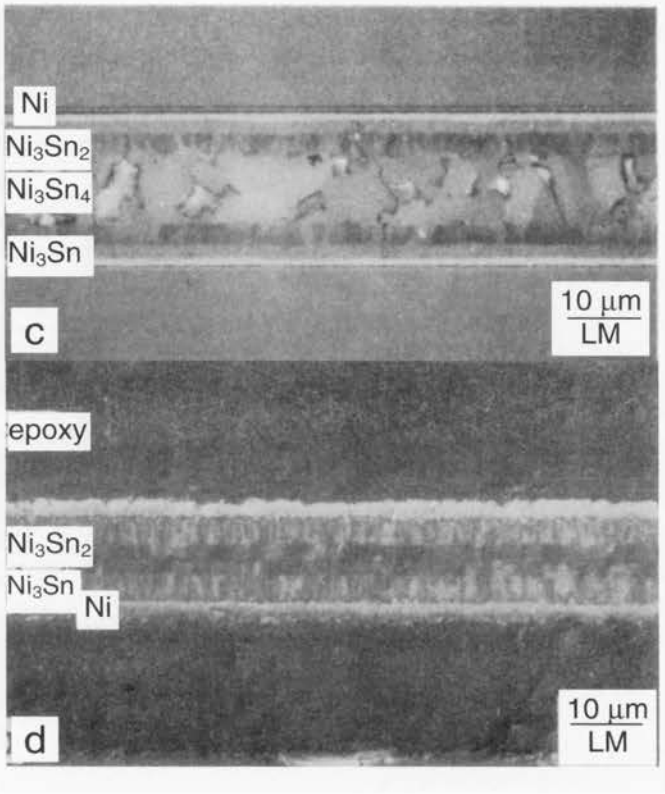

Fig. 15c-d. Ni/8.6 µm Sn/Ni interconnection after after 50.5 h (c) and 125 h (d) of reaction at 400 °C [15].

However, even long-term annealing at 400 °C (up to 125 h) did not result in a single IP present in the Ni/Sn/Ni joint [15]. The single IP is the most desired from the point of thermal stability of the joint as this enables to avoid the problem of microcracks or fissures in the interconnection zone.

In such a case, the tensile strength increases with the number of temperature cycles between 25 and 500 °C, from 25 (for 100 cycles) to 60 MPa (after 300 cycles) [25]. The thermal expansion coefficients of the IPs formed in the Ni/Sn/Ni joint are between that of the substrate and the filler material so that the joint behaves more likely as a graded one and little stress is expected due to thermal expansion mismatch.

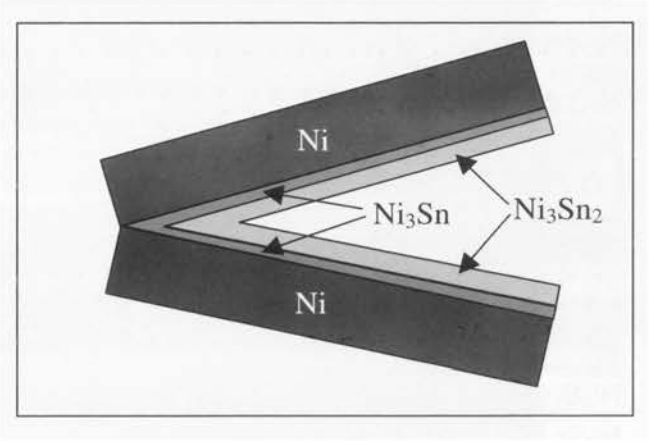

Fig. 16. Scheme of the sample destruction during the tensile strength test.

4.6. Ni/Al/Ni interconnection

The Ni-Al equilibrium phase diagram is presented in Fig. 17. At temperature slightly above the melting temperature of Al (660 °C), several intermetallic phases are formed, namely Al_3Ni, Al_3Ni_2, AlNi and $AlNi_3$. They are thermodynamically stable up to 854, 1133, 1638 and 1360 °C, respectively.

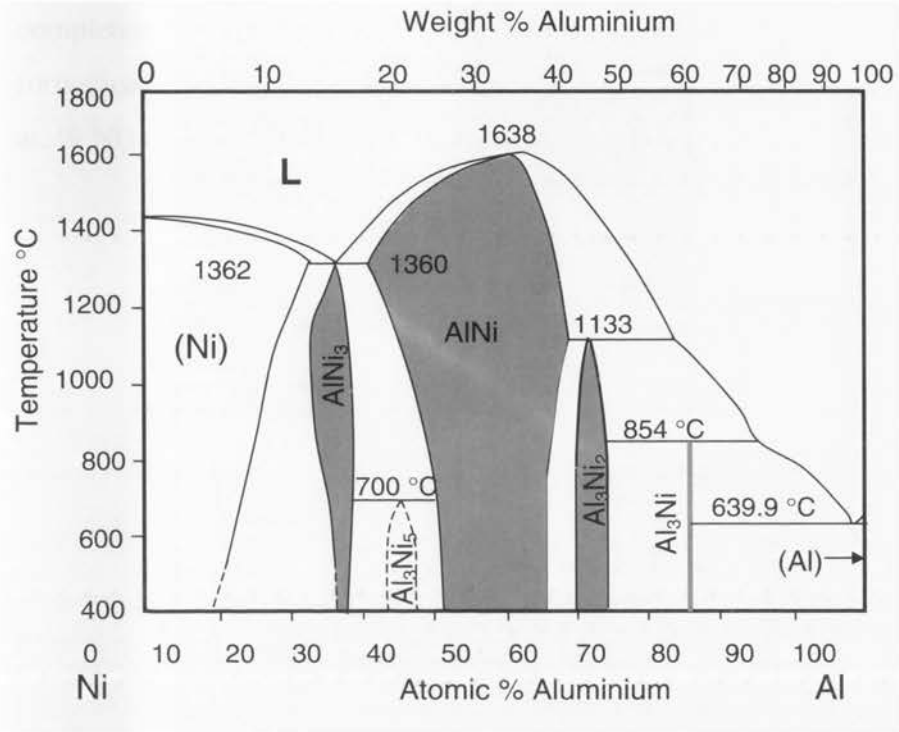

Fig. 17. The simplified version of Ni-Al equilibrium phase diagram based on data of Okamoto [26]

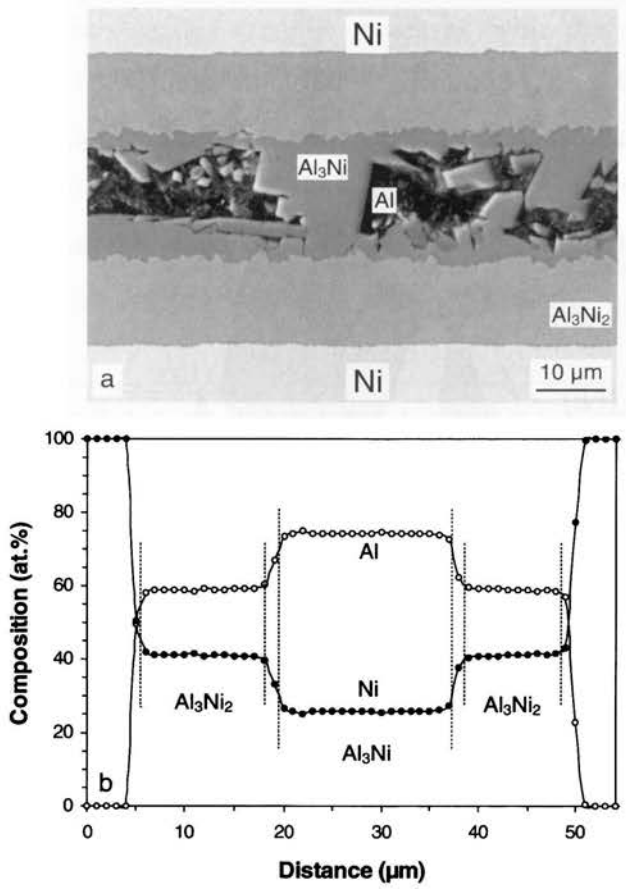

Fig. 18. SEM micrograph of the cross-sectional view of a Ni/Al/Ni interconnection after 2 min of reaction time at 720 °C (a) and corresponding electron probe line-scans for Al and Ni (b)

The Ni/Al/Ni bonds were accomplished due to isothermal solidification and subsequent interdiffusion of Ni and Al in the samples held at 720 °C [11, 27]. The formation of Ni/Al/Ni joint started from the reaction of liquid Al with solid Ni to form Al_3Ni intermetallic phase (Fig. 18). The reaction was very fast so that after 2 min of annealing Al_3Ni_2 was also

present in the joint in spite of the fact that a part of liquid Al has not been completely consumed. Further annealing at 720 °C resulted in the formation of two variants of the NiAl phase, namely a Ni-rich zone (60 at. % Ni) and stoichiometric AlNi (Fig. 19).

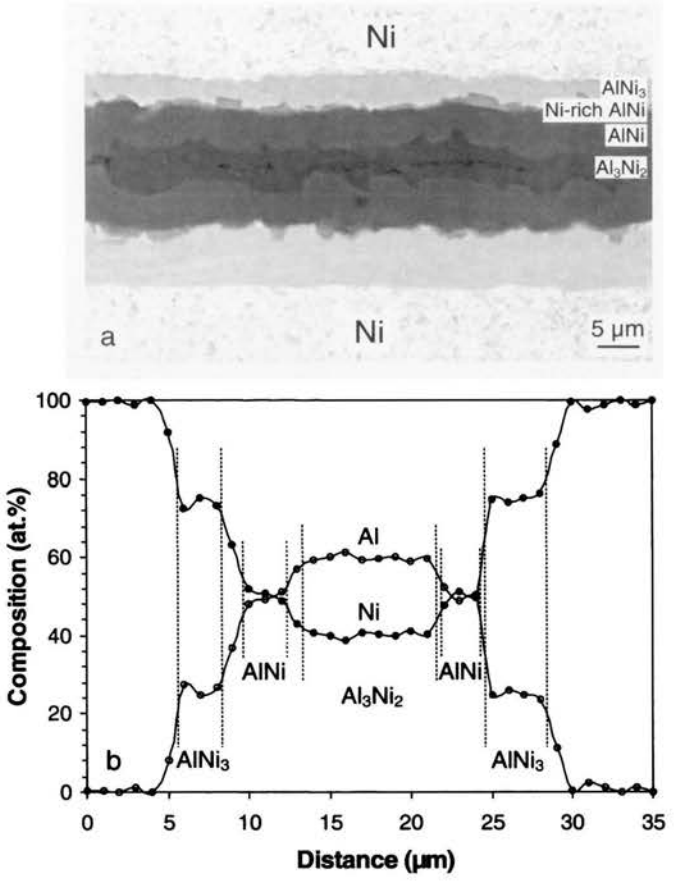

Fig. 19. SEM micrograph of the cross-sectional view of a Ni/Al/Ni interconnection after 20 min of reaction time at 720 °C (a) and corresponding EDX line-scans for Ni and Al (b)

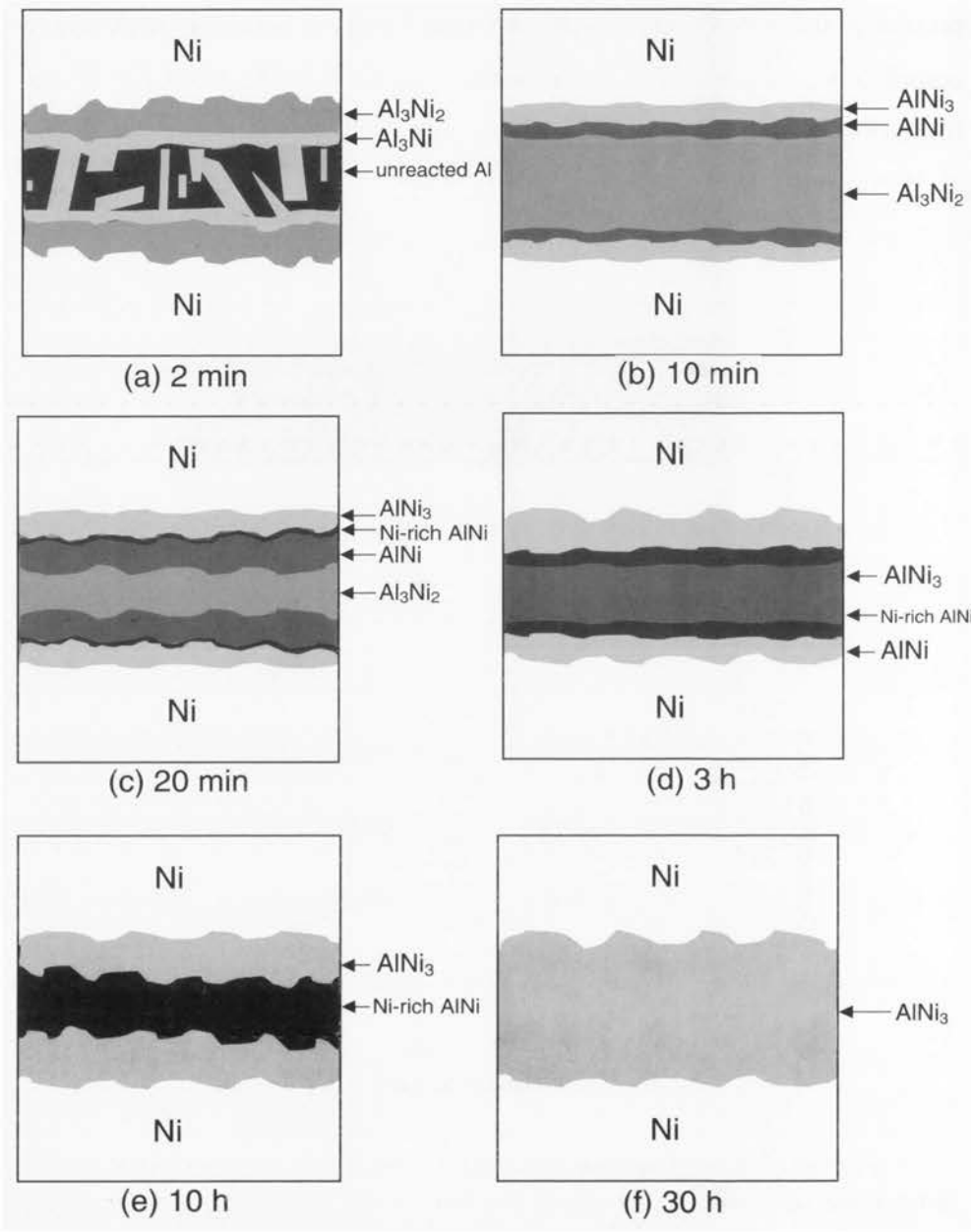

Fig. 20. Schematic representation of the sequence appearance of the Ips in Ni/Al/Ni interconnection obtained by diffusion soldering

The joining process was completed after 30 h of reaction with solely $AlNi_3$ compound to be present in the Ni/Al/Ni interconnection zone. Figure 20 is the schematic presentation of the sequence of phase appearance in Ni/Al/Ni interconnection. It can be summarized by the sequence:

$$\text{liquid Al} \rightarrow Al_3Ni \rightarrow Al_3Ni_2 \rightarrow \text{AlNi (stoichiom.)} \rightarrow \text{AlNi (Ni-rich)} \rightarrow AlNi_3.$$

In the intermediate stages even four intermetallic phases can exist simultaneously (see Fig. 20c and d).

5. Concluding remarks

The intermetallic phases can be considered as desirable and stable product of diffusion soldering process. This joining method combines the advantages conventional soldering (good joint filling and tolerance to surface preparation) and diffusion bonding (higher service temperature, smaller thermal expansion mismatches stresses). The intermetallics formed due to conventional soldering are limited only to the thin area adjacent to the substrate while joint interior is filled with starting solder material. Then, during service or even storage uncontrolled growth of existing or formation of new intermetallics can occur leading to the degradation of the joint quality. On the contrary, in diffusion soldering technology intermetallics fulfill all the interconnection area in the form of rather homogenous layer(s) and their growth is fully controlled during the production. Among the most important features are the higher thermal

stability (Fig. 21) and better mechanical properties (tensile and shear strength) than for conventional soldered joints (Fig. 22). So far, several systems have been successfully applied: Ag-In and Ag-Sn, Ni-Sn, Cu-Sn, Au-In, Au-Sn, Cu-In, Sn-In and Ni-Al. These interconnections can be used in electronic and electric devices (high temperature stable contacts of resistive heaters for thick-film hot plates, resistive elements for gas sensors, selective-area sealing and complete package sealing of microcircuits, development of packages for optoelectronics and other microcircuit application, wafer-to-wafer joining, flip-chip joining, 3D integration etc., producing metal-polyethylene interconnection).

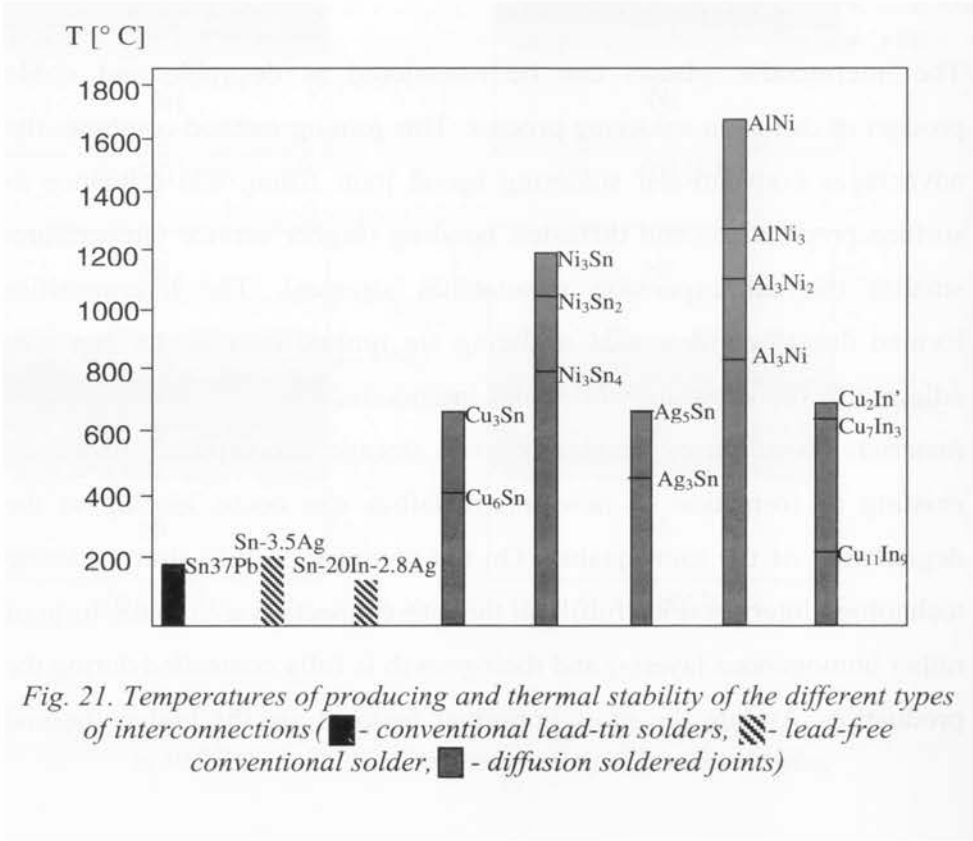

Fig. 21. Temperatures of producing and thermal stability of the different types of interconnections (■ - conventional lead-tin solders, ▨ - lead-free conventional solder, ■ - diffusion soldered joints)

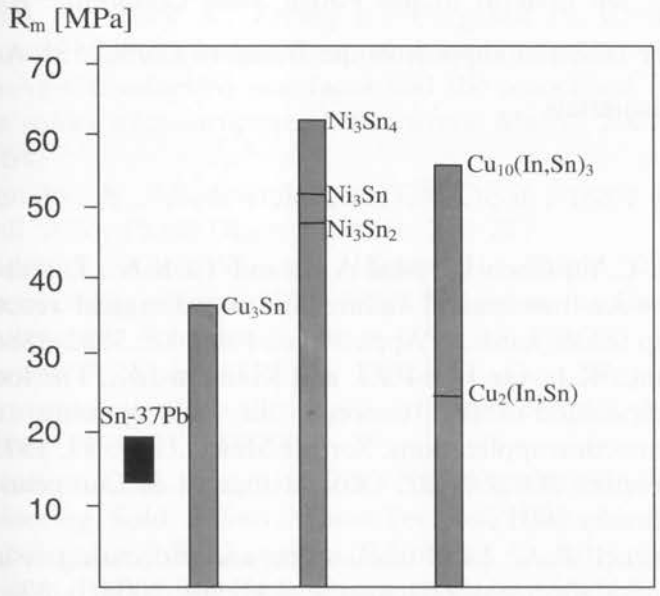

Fig. 22. Tensile strength of different types of interconnections (■ - conventional lead-tin solders, ■ - diffusion soldered joints). Based on Ref. [16, 25, 28]

The obtained intermetallic phases are also considered to be environmental-friendly materials which could replace hazardous conventional Pb-Sn solders. "COST 531 – Lead-Free Solder Materials" is European Action focus on the researching and designing new materials as perspective candidates for joining technology.

Acknowledgement

The authors are grateful to the Polish State Committee for Scientific Research for financial support in the frame of COST 531 Action- Lead free solder materials

References

1. Liu C.Y., Chen C., Mal A.K. and Tu K.N.: Direct correlation between mechanical failure and metallurgical reaction in flip chip solder joints. J. Appl. Phys., 1999, 85, 3882-3886.
2. Rönkä K.J., van Loo F.J.J. and Kivilahti J.K.: The local nominal composition-useful concept for microjoining and interconnection applications. Scripta Mater. 1997, 37, 1575-1581.
3. Directive 2002/95/EC, Official Journal of European Union (13 February 2003).
4. Fournell R.A.: Lead-free solders and processing issues relevant to microelectronics packaging. J.Metals, 2004, 6, 33.
5. Abtew A., Selvaduray G.: Lead-free solders in microelectronics. Mater. Sci. Eng. 2000, R 27, 95-141.
6. Humpsten G., Jacobson D.M.: Principles of soldering and brazing. 1993, ASM International, Materials Park, OH.
7. Khanna P.K., Dalke G., Gust W.: Morphology and long term stability of Ni/Ni interconnections based on diffusion soldering. Z. Metallkd. 1999, 90, 722-726.
8. Gale W.F.: Applying TLP bonding to the joining of structural intermetallic compounds. J. Metals, February 1999, 49-52.
9. Khanna P.K., Sommadossi S., Lopez G., Bielańska E., Zięba P., Chang L.S., Gust W., Mittemeijer E.J.: Development of Cu/Cu joints using an In interlayer. EUROMAT 1999, 214-218.
10. Zięba P., Wojewoda J.:Application of diffusion soldering in lead-free interconnection technology. Recent research developments in materials science. 2003, 4, 261-282.
11. Lopez G.A., Sommadossi S., Gust W., Mittemeijer E.J., Zięba P.: Phase characterization of diffusion soldered Ni/Al/Ni interconnections, Interface Sci. 2002, 10, 13-20.

12. Yang S.T., Chung Y., Kim Y.-H.: J. Microelectronics and Packaging Society, 2002, 9, 6
13. Zribi A., Clark A., Zaralij L., Borgesen P., Cotts E.J.: The growth of intermetallic compounds at Sn-Ag-Cu solder/Cu and Sn-Ag-Cu solder/Ni interfaces and the associated evolution of the solder microstructure. J. Electronic Mater., 2001, 20, 1157-1164.
14. Saunders N., Miodownik A.P.: The Cu-Sn (copper-tin) system. Bull. Alloy Phase Diagr. 1990, 11, 278-287.
15. Bader S., Gust W. and Hieber H.: Rapid formation of intermetallic compound by interdiffusion in the Cu-Sn and Ni-Sn systems. Acta Metall. Mater. 1995, 43, 329-337.
16. Bartels F., Morris J.W, Jr, Dalke G., Gust W.: Intermetallic formation of thin solid-liquid diffusion couples. J. Electronic Mater. 1994, 23, 787-790.
17. Jacobson D.M., Sangha S.P.S.: Novel applications of diffusion soldering. Sold. & Surf. Mount Technol, 1996., 23, 12-15.
18. Subramanin P.R., Laughlin D.E.: The Cu-In (copper-indium) system. Bull. Alloy Phase Diagr. 1989, 10, 555-568.
19. Lityńska L., Wojewoda J., Zięba P., Faryna M., Gust W., Mittemeijer E.J.: Characterization of interfacial reactions in Cu/In/Cu interconnections. Mikrochimica Acta 2004, 145, 107-110.
20. Sommadossi S., Lityńska L., Zięba P., Gust W., Mittemeijer E.J.: Transmission electron microscopy investigation of the microstructure and chemistry of the Si/Cu/In/Cu/Si interconnections. Mat. Chem. Phys. 2003, 81, 566-568.
21. Wang S.Q.: Barriers against copper diffusion into silicon and drift through silicon dioxide, MRS Bulletin XIX 1994, 30-40.
22. Elding-Ponten M., Stenberg L., Lidin S.: The η-phase field of the Cu-In system, J. Alloys and Comp. 1997, 261, 162-171.
23. Massalski T.B., Subramanian P.R., Okamoto H., Kasprzak L.: The Bi-In (Bismuth-Indium) system, Binary Alloys Phase Diagrams, 2nd ed., vol.1, ASM International, Materials Park, OH, 1990.
24. Nash P., Nash A.: The Ni-Sn (Nickel-Tin) system. Bull. Alloy Phase Diagr. 1985, 6, 350-358.

25. Khanna P.K., Dalke G., Gust W.: Morphology and long term stability of Ni/Ni interconnections based on diffusion soldering. Z. Metallkd. 1999, 90, 722-726.
26. Okamoto H.: Al-Ni (aluminium-nickel). J. Phase Equilibria 1993, 14, 257-259.
27. Lopez G., Zięba P., Sommadossi S., Gust W., Mittemeijer E.J.: Kinetic behaviour of diffusion-soldered Ni/Al/Ni interconnections. Mater. Chem. Phys. 2003, 78, 459-463.
28. Sommadossi S., Huci J., Khanna P.K., Gust W., Mittemeijer E.J.: Mechanical properties of Cu/in-48Sn/Cu diffusion-soldered joints. Z. Metallkd. 2002, 93, 496-501.